Bull. Mater. Sci. (2018) 41:93
https://doi.org/10.1007/s12034-018-1612-4

Synthesis and characterization of hydroxyapatite/alumina ceramic nanocomposites for biomedical applications

S VIGNESH RAJ[1], M RAJKUMAR[2,*], N MEENAKSHI SUNDARAM[3] and A KANDASWAMY[1]
[1]Department of Biomedical Engineering, PSG College of Technology, Coimbatore 641004, India
[2]Department of Physics, PSG College of Arts and Science, Coimbatore 641014, India
[3]Department of Physics, LRG Government Arts College for Women, Tiruppur 641604, India
*Author for correspondence (vmanirajkumar@gmail.com)

MS received 13 July 2017; accepted 17 November 2017; published online 6 July 2018

Abstract. In the present work, nanocrystalline hydroxyapatite/alumina ($HAp-Al_2O_3$) composite was prepared under specially designed stir-type hydrothermal reactor. The composite was prepared at two different temperatures under autogenous pressure and analysed for crystallinity, size, shape, composition and thermomechanical stability. The electron microscopy study shows the formation of $HAp-Al_2O_3$ composite nanorods with uniform distribution. The thermogravimetry analysis reveals better thermomechanical property with minimal weight loss at increased temperature. The effect of different concentrations of $HAp-Al_2O_3$ composite powders against MG63 human osteosarcoma cell lines shows excellent compatibility (80%) at high concentration of 200 $\mu g\ ml^{-1}$. These studies facilitate the formation of biocompatible $HAp-Al_2O_3$ composite nanorods for biomedical applications.

Keywords. Hydrothermal; hydroxyapatite; alumina; composite; biocompatibility.

1. Introduction

Hydroxyapatite (HAp) is the major mineral component of human bone and dentin in hierarchical arrangement with organic collagen fibrils. Synthetic hydroxyapatite has identical structural similarity with natural apatite. But due to its brittleness and low mechanical stability, reinforcement of polymers, metals and ceramics along with HAp to form a biocomposite has received much attention in the field of newer biomedical materials research [1]. Reinforcement of metal oxide ceramics such as ZrO_2, TiO_2 and Al_2O_3 at different stoichiometric ratios with pure hydroxyapatite enhance the mechanical stability and bone-like apatite formation [2]. Among the above reinforced materials, Al_2O_3-loaded HAp shows better mechanical stability and biocompatibility with surrounding cells and tissues. The incorporation of inert metal oxides such as Al_2O_3 acts as crack arresters and increases the mechanical strength of the hydroxyapatite composites [3,4]. Furthermore, addition of alumina into hydroxyapatite increases the compressive and bending strength of the composites [5–7]. Also, the *in vitro* compatibility evaluation of $HAp-Al_2O_3$ nanocomposites prepared under microwave-assisted synthesis and co-precipitation method shows similar biochemical activity like natural hydroxyapatite in bone. The bio-inertness of alumina has no harmful effect on cells and tissues [8,9]. Several methods were employed to synthesis $HAp-Al_2O_3$ composites such as sol–gel [10], co-precipitation method [11], ball mill [12], under-water shock compaction [13], protein-foaming consolidation method [14] and microwave-assisted preparation [15]. Based on the literature study, no hydrothermal experimental procedure was reported on the preparation of $HAp-Al_2O_3$ nanocomposites. Since, hydrothermal synthesis favoured the formation of tunable nanostructures of hydroxyapatite [16] and metal oxides with uniform morphological distribution [17], in the present work, $HAp-Al_2O_3$ nanocomposite prepared under stir-type hydrothermal process. The prepared composite powders were examined for structural, morphological, elemental and thermal analyses. Also, the biocompatibility of the prepared nanocomposite was studied against MG63 human osteosarcoma cell lines using MTT assay. The change in cellular morphology was also investigated under optical microscope.

2. Materials and methods

2.1 *Materials*

The analytical grade calcium nitrate tetrahydrate $(CaNO_3) \cdot 4H_2O$, diammonium hydrogen phosphate $(NH_4)_2HPO_4$ and aluminium nitrate $Al(NO_3)_2 \cdot 9H_2O$ reagents were used as starting materials for the preparation of $HAp-Al_2O_3$ composite. Twenty-five percent of ammonia solution was added to adjust pH of the reaction. All the chemicals purchased from Merck were used without any further purification. The stir-type hydrothermal vessel is designed and assembled at Amar equipments, Mumbai, India.

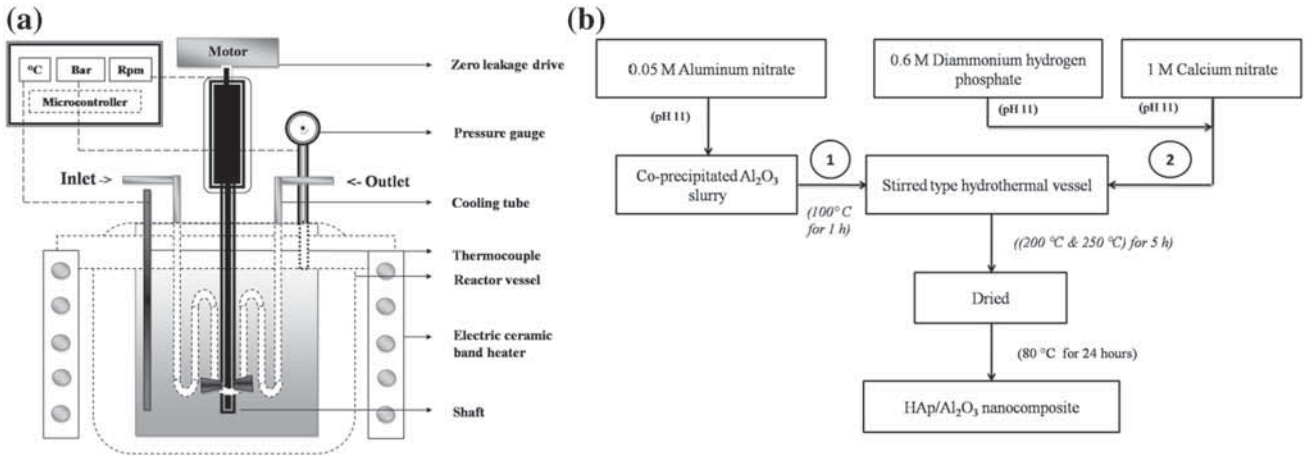

Figure 1. (**a**) Schematic representation of stir-type hydrothermal instrument and (**b**) flowchart for the synthesis of HAp−Al_2O_3 composite.

2.2 *Preparation of pure hydroxyapatite nanoparticles*

Pure hydroxyapatite nanoparticles were prepared using stir-type hydrothermal vessel with a stoichiometric ratio of 1.67 of calcium and phosphate precursors. The calcium nitrate and diammonium hydrogen phosphate solutions were prepared. Ammonia solution (25%) was used to adjust pH of the solutions to 11. The phosphate solution was added drop-wise to calcium solution and mixed well in a specially designed continuously stirred-type hydrothermal vessel shown in figure 1a. The mixed solution was hydrothermally treated at 250°C for 3 h under autogenous pressure (3.25 MPa). A steady stirring of 300 rpm was maintained throughout the reaction. After completion of the reaction, the white slurry was transferred to a beaker and washed three times with deionized water. The obtained powder was dried in hot air oven at 80°C for 24 h. After drying, the sample was calcined at 700°C for 3 h and powdered well using agate mortar and pestle.

2.3 *Preparation of HAp−Al_2O_3 composites*

The nanocomposite of HAp−Al_2O_3 was prepared by two stage synthesis such as co-precipitation and hydrothermal methods. Initially, hydroxyapatite and alumina nanoparticles were synthesized using hydrothermal and co-precipitation methods, respectively. The detailed process steps are illustrated in figure 1b. The hydrothermal reaction was carried out in a specially designed stirred-type hydrothermal reactor. The overnight precipitated alumina slurry prepared from aluminium nitrate (0.05 M) solution (pH 11) was transferred to hydrothermal vessel and subjected to hydrothermal treatment at 100°C for 1 h. After the completion of reaction, the reactor is cooled to 50°C with a cooling rate of 2°C per minute. Simultaneously, 0.1 M calcium nitrate and 0.06 M diammonium hydrogen phosphate were prepared with the stoichiometric ratio of Ca/P at 1.67.

When the initial hydrothermal reaction conditions were completed, the freshly prepared hydroxyapatite precursor solutions were transferred to the same hydrothermal vessel containing slurry of alumina. The pH of the solutions was maintained at 11 by ammonia solution. Finally, the reaction mixture containing alumina, calcium and phosphate solutions were subjected to hydrothermal treatment at 200−250°C for 5 h followed by natural cooling to room temperature. After the completion of hydrothermal process, the slurry containing both alumina and hydroxyapatite materials were transferred to a beaker and washed four times with deionized water. Then, the composite powders were dried at 80°C in a hot air oven and the samples powders were crushed well using agate mortar. The dried powders were kept in an air tight container and stored in a vacuum desiccator.

3. Characterization

The crystallographic analyses such as phase and crystallite size were determined through X-ray diffraction (XRD) pattern using PAN Analytical (The Netherlands), X'pert powder diffractrometer with 1.5406 Å CuK α radiation. The vibration and stretching bands of the IR absorption spectra were measured using Shimadzu, Fourier transform infrared (FTIR) spectrometer, Japan. The morphological and elemental compositions of the prepared samples were analysed using high-resolution transmission electron microscope (HRTEM) with energy-dispersive X-ray spectroscopy (EDS) (JEOL JEM 2100, Germany). Elemental mapping of the prepared composites was analysed using field-emission scanning electron microscope (FESEM) using Bruker, Germany. The specific surface area and the porosity were measured using Brunauer–Emmett and Teller (BET) and Barrett, Joyner and Halenda (BJH) techniques, respectively. The cytotoxicity study was performed using MTT assay against MG63 human osteosarcoma cell lines obtained from National Centre for Cell Science (NCCS), Pune, and grown in Eagle's minimum essential medium containing 10% foetal bovine serum (FBS). The cells were maintained at 37°C, 5% CO_2, 95% air and 100% relative

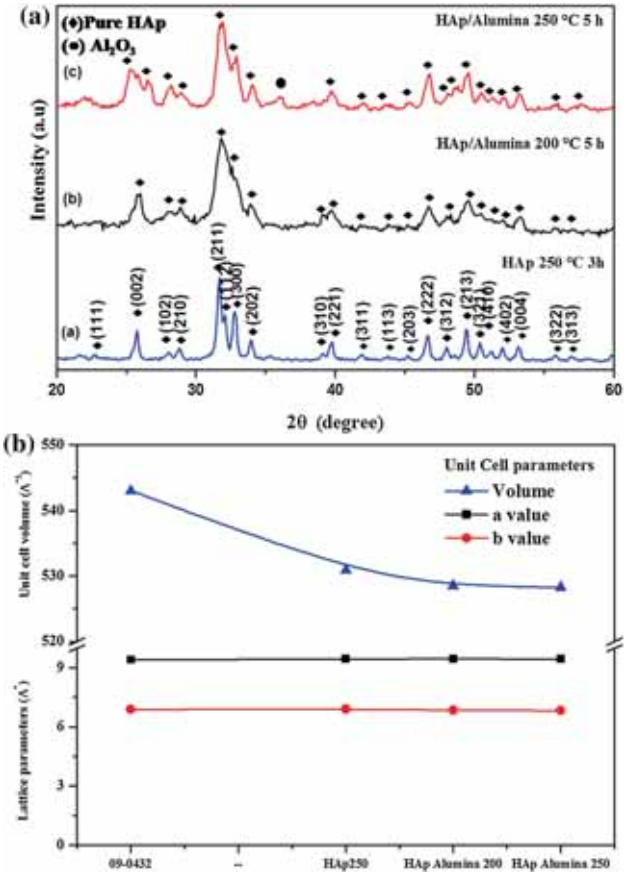

Figure 2. (**a**) XRD pattern and (**b**) unit cell parameters/volume of hydrothermally prepared pure HAp and HAp−Al_2O_3 composite.

humidity in a CO_2 incubator. The cultures were passaged weekly, and the culture medium was changed twice in a week.

4. Results and discussion

4.1 *XRD*

The XRD patterns of pure HAp and HAp−Al_2O_3 composites prepared under hydrothermal conditions are shown in figure 2a. Major diffracted peaks match well with the published HAp (JCPDS file no. 09-0432). Besides, the characteristic peak (102) of θ-Al_2O_3 was observed at 35.9° (2θ) for the sample treated at 250°C for 5 h, peak broadening was observed around 25−35° (2θ) caused by the overlapping of θ-Al_2O_3 (JCPDS file no. 23-1009) peaks with HAp peaks in both the samples.

The average crystallite size was calculated using Scherrer's equation. The relation between interplanar spacing (d), unit cell parameters (a, c) and miller indices (h, k, l) of the hexagonal crystal system (hydroxyapatite) are expressed as [18],

$$\frac{1}{d^2} = \frac{4}{3}\left(\frac{h^2 + hk + k^2}{a^2}\right) + \frac{l^2}{c^2}. \quad (1)$$

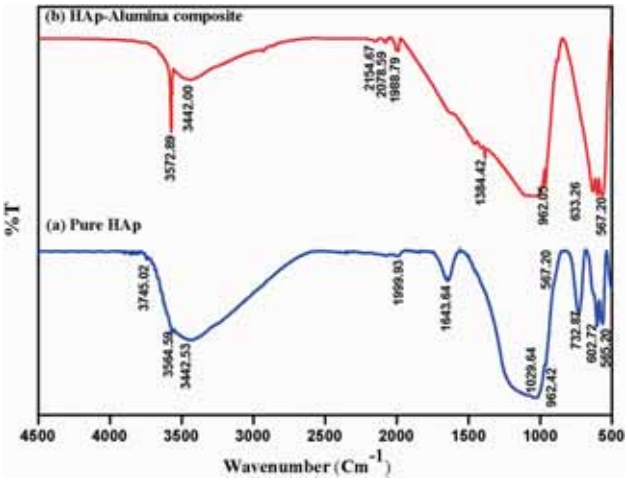

Figure 3. FTIR spectrum of hydrothermally prepared (**a**) pure HAp and (**b**) HAp−Al_2O_3 composite.

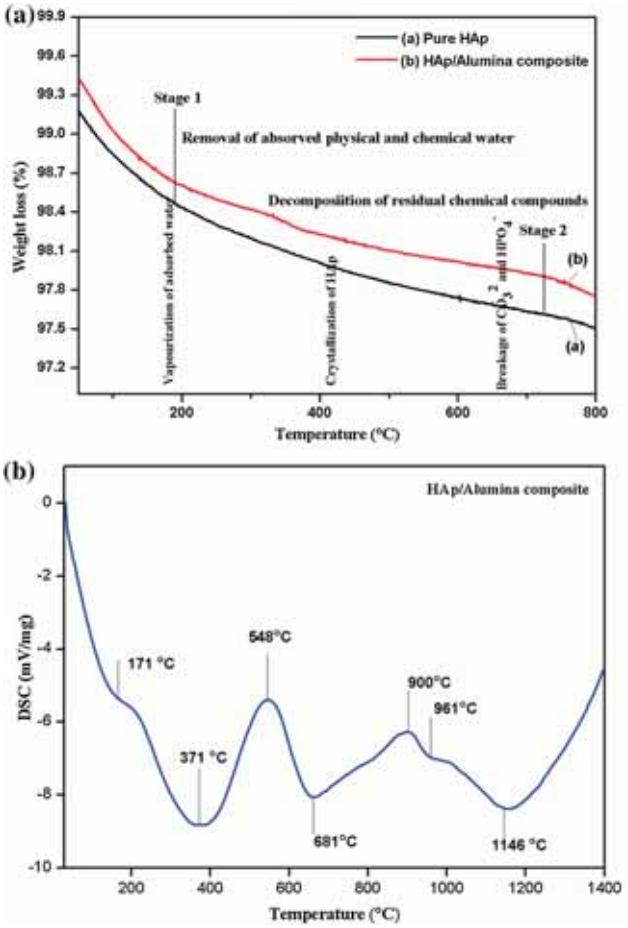

Figure 4. (**a**) TG curves of pure HAp and HAp−Al_2O_3 composite and (**b**) DSC curve of hydrothermally prepared HAp−Al_2O_3 composite.

Based on the XRD data, average crystallite size, the lattice parameters (a, b, c) and volume (V) were calculated for

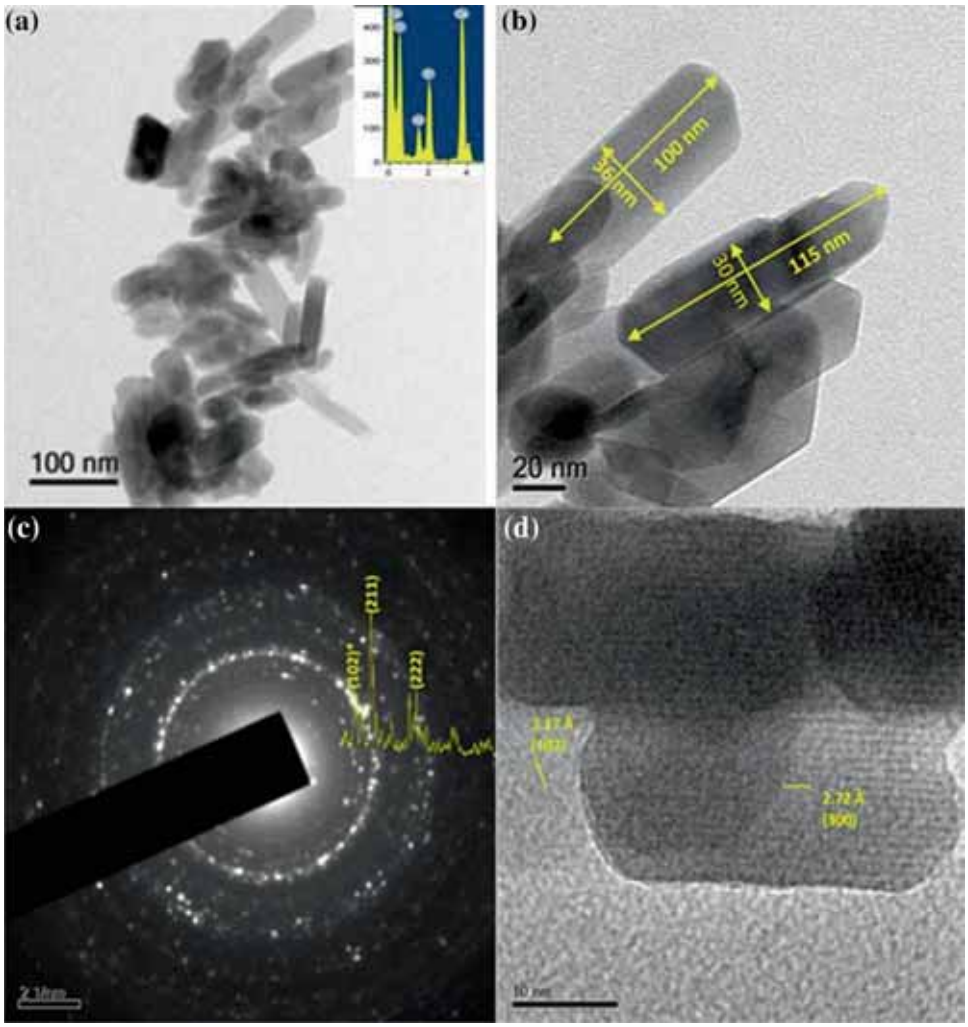

Figure 5. (**a**) TEM image with EDS, (**b**) TEM-nanorods, (**c**) SAED pattern, and (**d**) HRTEM image of HAp−Al_2O_3 composites hydrothermally prepared at 250°C for 5 h.

hexagonal crystal system of HAp and HAp−Al_2O_3 composites.

The average crystallite size of synthesized pure HAp is 41.3 nm, whereas HAp−Al_2O_3 composites are calculated as 9.6 and 14.6 nm. The reduction in the crystallite size is due to the presence of Al_2O_3, which prevent the fusion of nucleated HAp particles. So, Al_2O_3 helps to prevent the particle agglomeration and maintain the particle size smaller for HAp−Al_2O_3 composite. This study is also in good agreement with the TEM analysis. The reduction of C-axis of unit cell and overall cell volume might be due to the diffusion of aluminium element into HAp structure, which perturbates the unit cell parameters of HAp crystal system as shown in figure 2b. The difference of Bohr atomic radius between calcium (194 pm) and aluminium (118 pm) contributes to the reduction in unit cell volume. Based on the XRD data, HAp−Al_2O_3 composite prepared at 250°C for 5 h shows better crystallinity, was considered for further analysis.

4.2 *FTIR*

The FTIR spectra of pure HAp and HAp−Al_2O_3 composite are shown in figure 3. The IR band peaks around 3745 and 633 cm^{-1} correspond to asymmetric OH stretching vibrations [19]. The peaks at 3564 and 3572 cm^{-1} related to the stretching modes of surface hydroxyl group and absorbed water, respectively [20]. The peaks observed at 2155, 2079, 1989 cm^{-1} related to moisture/CO_2 absorption [21] and 1644 cm^{-1} corresponds to lattice water [22]. The IR band peaks observed at 1033, 1072 (V_3), 962 (V_1) and 562 cm^{-1} (V_4) correspond to asymmetric stretching and bending vibration of PO_4^{3-} group [24–26].

4.3 *TGA*

The thermogravimetric analysis (TGA) curve of pure HAp and HAp−Al_2O_3 nanocomposite shown in figure 4a, clearly indicates the weight loss around 3% for pure HAp and

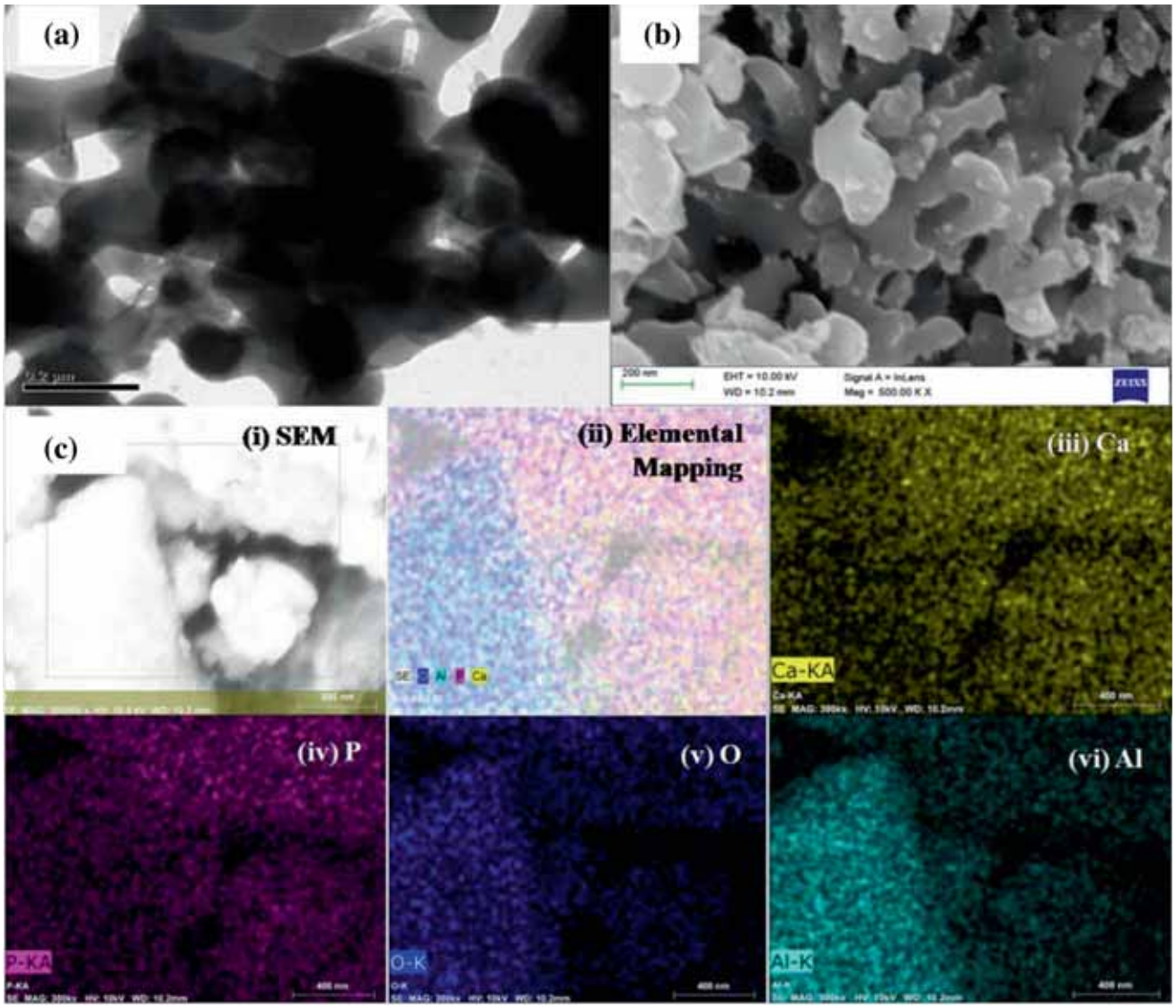

Figure 6. (**a**) TEM image, (**b**) FESEM image, and (**c**) elemental mapping of hydrothermally prepared HAp−Al_2O_3 composite calcined at 900°C for 3 h.

HAp−Al_2O_3 nanocomposite. Also, minimal weight loss in the HAp−Al_2O_3 composite compared to pure HAp might be due to the addition of alumina. The removal of water molecules and decomposition of residual chemical compounds constitute 3% weight loss upon thermal treatment [27,28]. The TGA curve provides valuable information on stability and thermal processing of prepared composite for bone implants.

Based on XRD and FTIR results, HAp−Al_2O_3 composite prepared at 250°C for 5 h shows better crystallinity and thermal property compared with pure HAp. Therefore, the composite powder was further analysed using differential scanning calorimetry (DSC), electron microscopy, nitrogen adsorption–desorption measurements and *in vitro* cytotoxicity study.

4.4 *DSC*

The thermal behaviour of the prepared HAp−Al_2O_3 composite was examined by DSC is shown in figure 4b. The peak at 171°C corresponds to the vapourization of solvent molecules. The peak at 371°C corresponds to the onset of Al_2O_3 crystallization removal of surface (NH_3 and water) and lattice (CO_3 and water) followed by crystallization of Al_2O_3 at 548°C [29]. Similarly, the peaks at 681 and 900°C favour HAp crystallization process, whereas the peaks at 961 and 1146°C indicate the secondary reactions between HAp and Al_2O_3 [30,31]. This result clearly illustrates the calcination process at 900°C (<1000°C) is effective for the formation of HAp−Al_2O_3 composite without any interfacial reactions.

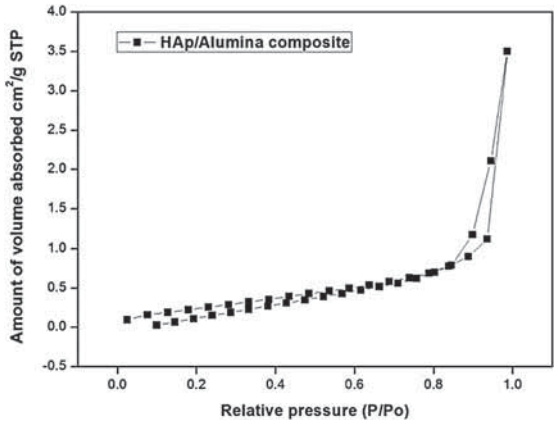

Figure 7. N_2 adsorption–desorption isotherms for $HAp-Al_2O_3$ composite.

4.5 *Electron microscopy analysis*

The TEM images of as-prepared composite powder prepared at 250°C for 5 h clearly indicates the formation of nanorods as shown in figure 5a. The prepared nanorods were 90–110 nm in length and 25–35 nm in width as shown in figure 5b. The selected area diffraction (SAED) pattern matches well with the XRD pattern of $HAp-Al_2O_3$ composite with the high intense peak of HAp (211) as shown in figure 5c. The HRTEM image shown in figure 5d reveals the d-spacing values at 3.17 and 2.72 Å that correspond to the crystallographic planes of (102) and (300) of HAp crystals, respectively.

Though the as-prepared nanocomposite exhibits one-dimensional rod-like morphology, the TEM micrographs of calcined (900°C for 3 h) $HAp-Al_2O_3$ nanocomposite (figure 6a) reveals the diffusion of rod morphology. Similarly, the FESEM micrograph shown in figure 6b clearly illustrates the formation of flake-like structures as a result of diffusion of rod

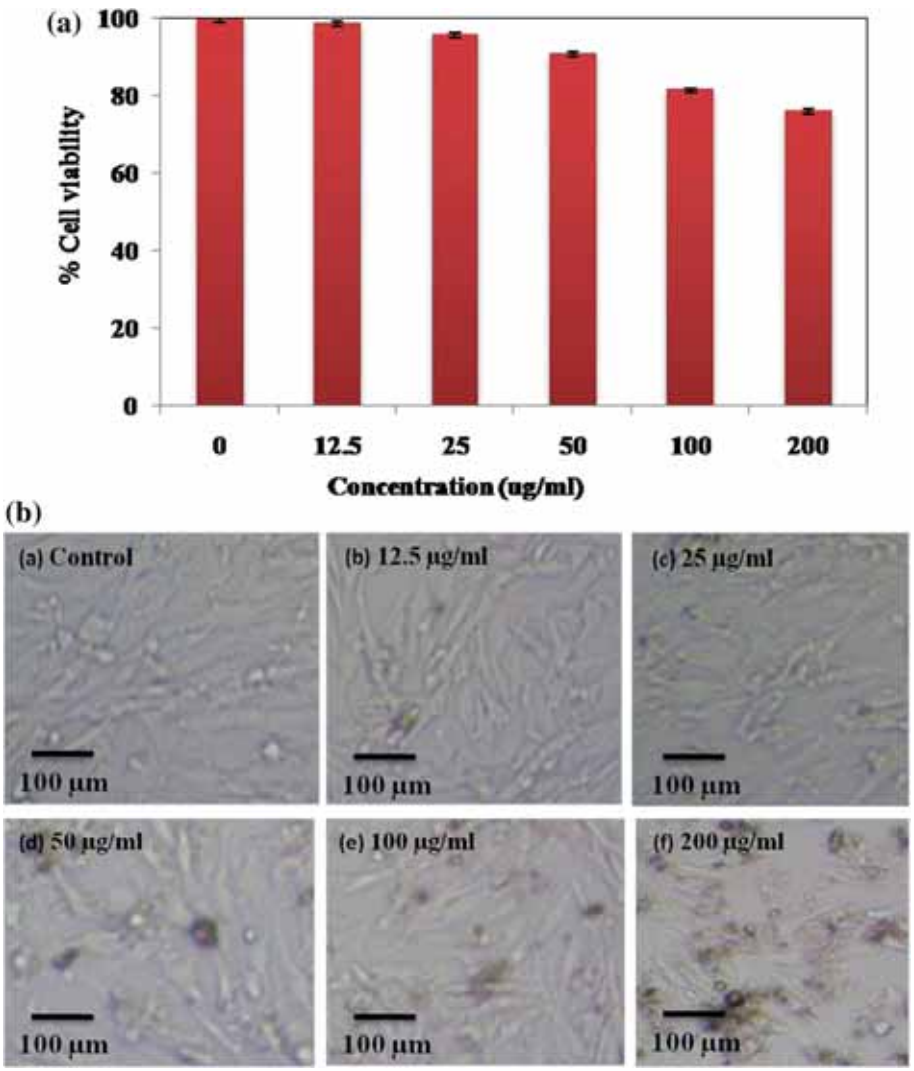

Figure 8. (**a**) MTT assay and (**b**) optical microscope images of $HAp-Al_2O_3$ composite against MG63 human osteoblasts-like cell lines.

structures. The dual time thermal processing (hydrothermal and calcination) of the sample might have caused the change in morphology of the prepared composite.

The elemental mapping analysis clearly reveals the uniform elemental distribution of Ca, P, O, Al as shown in figure 6c(ii). The dense distribution of calcium (Ca) in figure 6c(iii) and phosphate (P) in figure 6c(iv) with sparsely disturbed oxygen (O) in figure 6c(v) confirms the presence of hydroxyapatite (HAp). Similarly, the distribution of Al and O in a particular region as shown in figure 6c(vi) and 6c(v) confirms the presence of alumina. The elemental mapping of hydrothermally prepared HAp−Al_2O_3 composite shows microstructures of HAp and Al_2O_3 separately, which is evident that no intermediate compounds are produced.

4.6 *Nitrogen adsorption–desorption measurements*

The N_2 adsorption isotherms of HAp−Al_2O_3 composite is shown in figure 7. The pore size and pore volume are calculated from BJH method of desorption isotherm. The composite exhibits typical type 3 isotherm curves and this type of adsorption isotherm occur with pores in the range of 1.5–100 nm [21]. The BET surface area was measured at low $P/P_o = 0.85$. The specific surface area, total pore volume and average pore radius are found to be 13.286 $m^2\ g^{-1}$, 6.283×10^{-3} cc g^{-1} and 1.703 nm, respectively.

4.7 *Cytotoxicity study*

The prepared nanocomposites are analysed for *in vitro* cytotoxicity activity using MTT assay against MG63 human osteoblast-like cell lines, which exhibits similar adhesiveness and physiology as that of human osteoblasts cells [31] and the morphology of osteosarcoma cells treated with different concentrations of HAp−Al_2O_3 nanocomposite powders are shown in figure 8. The percentage cell viability for different concentrations of HAp−Al_2O_3 nanocomposite is observed around 80% at maximum concentration (200 $\mu g\ ml^{-1}$) as shown in figure 8a. It is quantitatively confirmed with no considerable change in the morphology of cells at higher concentration under optical microscope, images are shown in figure 8b. Thus, MTT assay clearly indicates that the prepared nanocomposite is highly compatible for orthopaedic applications.

5. Conclusion

In this study, HAp−Al_2O_3 composites were successfully prepared using stirred-type hydrothermal reactor at 250°C for 5 h under autogenous pressure. It was observed that the increase in reaction temperature favours the formation of nanocrystalline HAp−Al_2O_3 biocomposite material. The electron microscopy analysis of the as-prepared nanocomposite reveals one-dimensional rod-like morphology in the size range of 100 nm in length and 30 nm in width. In addition, the calcined HAp−Al_2O_3 composite exhibit good thermal stability with only 3% weight loss that favours the processing of these ceramic composites for bone substitutes. Further, the materials' excellent compatibility against MG63 human osteoblasts-like cells ensures its use in biomedical applications, especially in the field of orthopaedics.

Acknowledgements

We are grateful to PSG institutions for providing necessary facilities to carry out the research. The author, S Vignesh Raj, is grateful to UGC National fellowship F./2014-15/NFO-2014-15-TAM-OBC-10405/ (SA-III website) for providing PhD assistantship. This work was financially supported by UGC MRP file. no. 42-867/2013 (SR).

References

[1] Supova M 2015 *Ceram. Int.* **41** 9203
[2] Mezahi F Z, Oudadesse H, Harabi A and Gal Y 2012 *Int. J. Appl. Ceram. Technol.* **9** 529
[3] Oktar F N, Agathopoulos S, Ozyegin L S, Gunduz O, Demirkol N, Bozkurt Y *et al* 2007 *J. Mater. Sci.: Mater. Med.* **18** 2137
[4] Evis Z and Doremus R H 2005 *Mater. Lett.* **59** 3824
[5] Jun Y K, Kim W H, Kweon O K and Hong S H 2003 *Biomaterials* **24** 3731
[6] Sanayei M, Nasiri-Tabrizi B, Ebrahimi-Kahrizsangi R and Shokuhfar A 2010 *J. Nano Res.* **11** 145
[7] Juang H Y and Hon M H 1994 *J. Mater. Sci. Eng. C* **2** 77
[8] Gautier S, Champion E and Bernache-Assollant D 1999 *J. Mater. Sci.: Mater. Med.* **10** 533
[9] Yelten A, Yilmaz S and Oktar F N 2012 *Ceram. Int.* **3** 2659
[10] Ramesh S, Natasha A N, Tan C Y, Bang L T, Niakan A, Purbolaksono J *et al* 2015 *Ceram. Int.* **41** 10434
[11] Kim S, Kong Y M, Lee I S and Kim H E 2002 *J. Mater. Sci.: Mater. Med.* **13** 307
[12] Hannora A E 2014 *J. Ceram. Sci. Technol.* **5** 293
[13] Chiba A, Kimura S, Raghukandan K and Morizono Y 2003 *J. Mater. Sci. Eng. A* **350** 179
[14] Sopyan I, Fadli A and Mel M 2012 *J. Mech. Behav. Biomed. Mater.* **8** 86
[15] Radha G, Balakumar S, Venkatesan B and Vellaichamy E 2015 *J. Mater. Sci. Eng. C* **50** 143
[16] Costa D, Dixon S J and Rizkalla A S 2012 *ACS Appl. Mater. Interf.* **4** 1490
[17] Labat B, Chamson A and Frey J 1995 *J. Biomed. Mater. Res.* **29** 1397
[18] Rajkumar M, Meenakshi Sundaram N and Rajendran V 2011 *Dig. J. Nanomater. Biostruct.* **6** 169
[19] Mujahid M, Sarfraz S and Amin S 2015 *Mater. Res.* **18** 468
[20] Zhang Y and Lu J 2008 *Cryst. Growth Des.* **8** 2101
[21] Nath S, Biswas K, Wang K, Bordia R K and Basu B 2010 *J. Am. Ceram. Soc.* **93** 1639
[22] Ribeiro C C, Gibson I and Barbosa M A 2006 *Biomaterials* **27** 1749
[23] Chen D Z, Tang C Y, Chan K C, Tsui C P, Peter H F, Leung M C *et al* 2007 *J. Comp. Sci. Tech.* **67** 1617

[24] Lak A, Mazloumi M, Mohajerani M, Kajbafvala A, Zanganeh S, Arami H *et al* 2008 *J. Am. Ceram. Soc.* **91** 3292
[25] Rhee S H and Tanaka J 2002 *J. Mater. Sci.: Mater. Med.* **13** 597
[26] Thomas V, Dean D R, Jose M V, Mathew B, Chowdhury S and Vohra Y K 2007 *Biomacromolecules* **8** 631
[27] Barakat N A, Khalil K A, Sheikh F A, Omran A M, Gaihre B, Khil S M *et al* 2008 *J. Mater. Sci. Eng. C* **28** 1381
[28] Sathyaseelan B, Baskaran I and Sivakumar K 2013 *Soft Nanosci. Lett.* **3** 69
[29] Kaur G, Pickrell G, Kimsawatde G, Homa D, Allbee H A and Sriranganathan N 2014 *Sci. Rep.* **4** 4392
[30] Zhang C, Zhang X, Liu C, Sun K and Yuan J 2016 *Ceram. Int.* **42** 279
[31] Pandey A K, Pati F, Mandal D, Dhara S and Biswas K 2013 *J. Mater. Sci. Eng. C* **33** 3923